ACS OMEGA

http://pubs.acs.org/journal/acsodf

Article

Thermodynamics of Azo Dye Adsorption on a Newly Synthesized Titania-Doped Silica Aerogel by Cogelation: A Comparative Investigation with Silica Aerogels and Activated Charcoal

Prashant D. Sarvalkar, Apurva S. Vadanagekar, Omkar S. Karvekar, Pramod D. Kumbhar, Santosh S. Terdale, Avinash Singh Thounaojam, Sanjay S. Kolekar, Rajiv S. Vhatkar, Pramod S. Patil, and Kiran Kumar K. Sharma*

Cite This: *ACS Omega* 2023, 8, 13285−13299

Read Online

ACCESS | Metrics & More | Article Recommendations | Supporting Information

ABSTRACT: The adsorption isotherms of azo dyes on a newly synthesized titania-doped silica (TdS) aerogel compared to silica aerogels and activated charcoal (AC) are systematically investigated. Monolithic TdS aerogels were synthesized by the cogelation process followed by supercritical drying of tetraethyl orthosilicate (TEOS) as a gel precursor and titanium(IV) isopropoxide (TTIP) as a metal complex precursor for copolymerization in ethanol solvent. An acid−base catalyst was used for the hydrolysis and condensation of TEOS and TTIP. The effect of Ti^{4+} doping in a silica aerogel on the mesoporous structure and the adsorption capacity of methylene blue (MB) and crystal violet (CV) dyes were evaluated from the UV−vis absorption spectra. In order to compare the adsorption isotherms, the surface areas of silica and TdS aerogels were first normalized with respect to AC, as adsorption is a surface phenomenon. The azo dye equilibrium adsorption data were analyzed using different isotherm equations and found to follow the Langmuir adsorption isotherm. The maximum monolayer adsorption capacities for the adsorbent TdS aerogel normalized with the AC of the Langmuir isotherm are 131.58 and 159.89 mg/g for MB and CV dyes, respectively. From the Langmuir curve fitting, the Q_{max} value of the TdS aerogel was found to increase by 1.22-fold compared to AC, while it increased 1.25−1.53-fold compared to the silica aerogel. After four cycles, regeneration efficiency values for MB and CV dyes are about 84 and 80%, respectively. The study demonstrates the excellent potential and recovery rate of silica and TdS aerogel adsorbents in removing dyes from wastewater. The pore volume and average pore size of the new aerogel, TdS, were found to be lower than those of the silica aerogel. Thus, a new TdS aerogel with a high capacity of adsorption of azo dyes is successfully achieved.

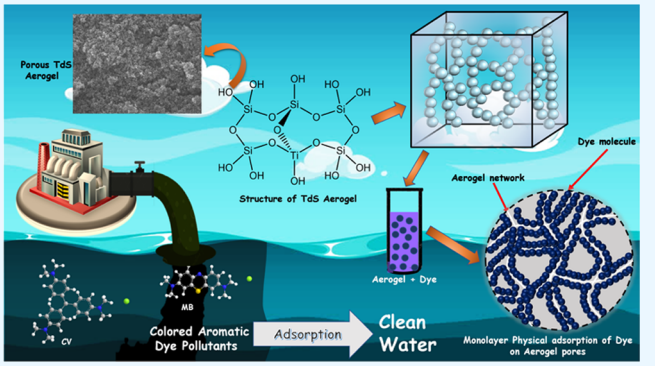

1. INTRODUCTION

The fast-growing textile and dyeing industries are currently causing a number of environmental challenges. In attempts to solve these problems, various methods like adsorption,[1] photocatalytic degradation,[2−5] flocculation,[6] electrochemical,[7] bioremediation,[8] ion exchange,[9] membrane filtration,[10] etc., are employed. Among these processes, adsorption proves to be the most efficient technology because of various factors such as its less complicated nature, ease of operation, low running cost, high retention potential, and regeneration efficiency.[11−15] A surface phenomenon known as "adsorption" occurs when a species gets accumulated on the surface of another phase, which is usually solid or liquid, by physical and/or chemical interactions. These materials on which the adsorption process takes place are known as adsorbents. The properties of these adsorbents vary significantly as a function of their surface area, size of particles, low rate of intraparticle diffusion and high adsorption capacities, and number of active surface sites.[16]

One drawback of this method is that the adsorbent to be used should have a smaller size, since nanosized mesoporous adsorbents have a high surface area, which results in high adsorption capacity. However, employing smaller adsorbents creates another problem. That is, the smaller absorbents are difficult to recover after they have reached their saturation adsorption capacity.[17] To overcome this problem, monolithic

Received: January 27, 2023
Accepted: March 17, 2023
Published: March 31, 2023

Scheme 1. Schematic Representation of the (a) Cogelation Process of the Synthesis of the Silica Aerogel and (b) Cogelation Process of the Synthesis of the TdS Aerogel

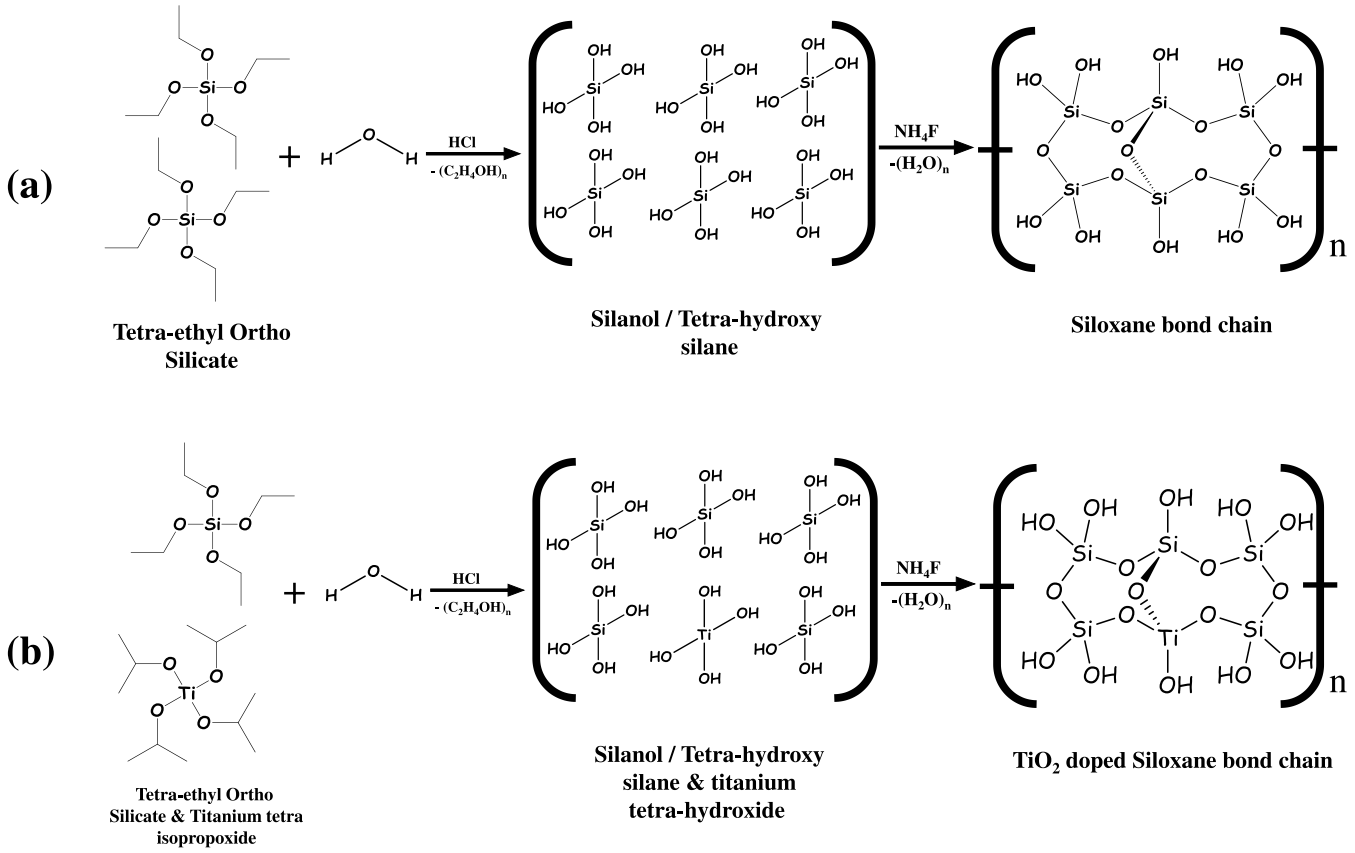

mesoporous aerogels are studied exhaustively around the globe for their applications in environmental remediation.

Aerogels contain 95−98% of air and the remaining part is a solid network structure.[18] Due to the low thermal conductivity, high porosity, mesoporous structure, low density, and transparency properties of aerogels, they are of interest for many potential applications including thermal insulation,[19] heavy metal or dye adsorption,[20] nanocatalysis,[21] drug delivery,[22] and different sensor technologies.[23] There are various ways of manufacturing aerogels, including supercritical, ambient, and freeze-drying methods.[24] Supercritical drying of aerogels results in a mesoporous structure.

Numerous researchers have proposed a synthesis process to change the physiochemical properties of aerogels in view of remarkable technical potential and rising environmental degradation. Most of the reported work on silica aerogels focuses on the development of effective thermal insulators, notably for the construction and aerospace industries. However, these applications have been restricted by the silica aerogel's poor mechanical characteristics or network fragility.[25] Although silica aerogels have received the most attention, their poor mechanical properties and hygroscopic (moisture-sensitive surface) nature have restricted their potential applications in aircraft, industry, and daily life.[26−28] In order to overcome these limitations, transition metal ion doping is reported to improve the mechanical property in the synthesis of metal-doped carbon xerogels using the cogelation process.[28]

Herein, we report the use of the cogelation process using the titanium isopropoxide (TTIP) inorganic complex as a Ti^{4+} source and tetraethyl orthosilicate (TEOS) as a gel precursor, co-polymerized using acid−base/ammonium fluoride as the catalyst followed by supercritical drying. A new Ti^{4+}-doped silica aerogel (TdS), a monolithic aerogel, of high mechanical strength is reported for the first time. The as-synthesized TdS aerogel was investigated as an adsorbent for the adsorption of methylene blue (MB) and crystal violet (CV), which are model azo dyes, and compared to the prepared silica aerogel and activated charcoal using adsorption isotherm models of Langmuir, Freundlich, and Temkin.

2. EXPERIMENTAL PART

2.1. Materials. Ammonium hydroxide (NH_4OH), activated charcoal (AC), ethanol (EtOH), hydrochloric acid (HCl), tetraethyl orthosilicate (TEOS), titanium tetraisopropoxide (TTIP), and methylene blue (MB) and crystal violet (CV) dyes are purchased from S.D. Fine Chemicals, Pune, (MH), India. All of the above reagents are analytical grade and used without any additional purification. Deionized water with a resistivity of 18.2 MΩ/cm from an ELGA system is used for the preparation of all of the solutions in the experiments.

2.2. Synthesis of Silica Aerogel. The silica gel was prepared by using a two-step acid−base-catalyzed sol−gel process. For the preparation of 36 mL of solution A, TEOS, EtOH, H_2O, and dil. HCl were taken and magnetically stirred for 12 h at room temperature to ensure complete hydrolysis of TEOS. However, the final molar ratio for silica sol was 1:1.25:9.56 for TEOS, H_2O, and EtOH, respectively. To increase the rate of hydrolysis of TEOS, 0.25 mL of 1 N HCl acid as a catalyst was added.

https://doi.org/10.1021/acsomega.3c00552
ACS Omega 2023, 8, 13285−13299

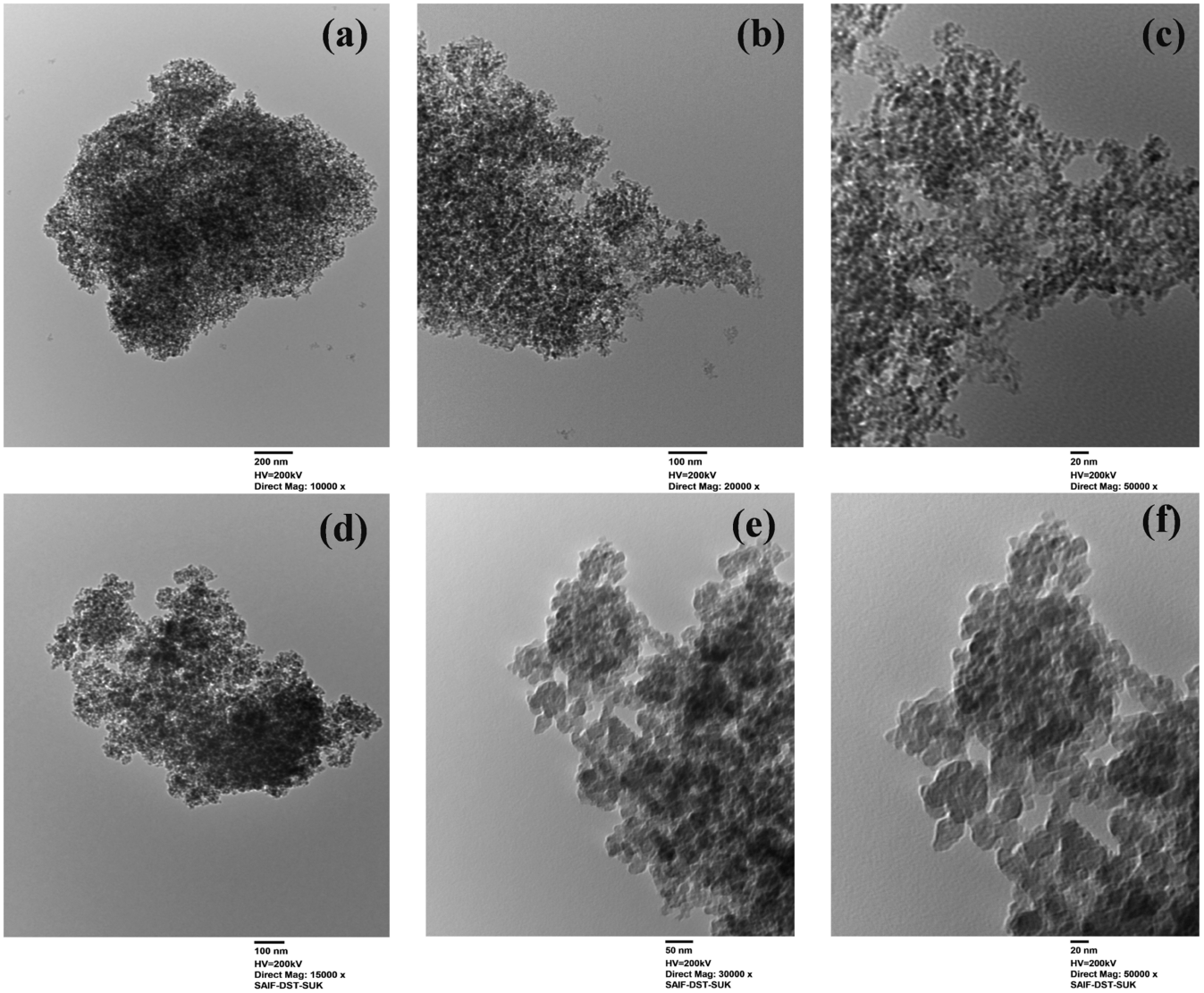

Figure 1. TEM images of (a–c) silica and (d–f) TdS aerogels.

In the second phase, 0.5 mL of 1 M NH_4F was added dropwise to solution A and stirred for 30 min. The sol was transferred into a quartz mold to set the gel. The developed sol was then agitated for 1 h, resulting in the formation of a transparent colloidal suspension. The gel was then formed in 24 h and aged in ethanol three times for 24 h intervals to exchange water and other solvents from the gel.

Later, the silica gel was transferred to a high-pressure and -temperature reactor. Ethanol filled one-third of the chamber. The aerogel was supercritically dried at 243°C and 63 bar.

The parameters affecting the process of hydrolysis and condensation (sol–gel) are TEOS reactivity, TEOS-to-water ratio, pH, temperature, solvent, and catalyst concentration. The process of hydrolysis contains the splitting of water molecules, i.e., H^+ and OH^- ions. The formation of the aerogel involves a colloidal solution (sol), followed by gelation, and drying of the gel by supercritical drying, i.e., at high temperature and pressure. The schematic representation of silica aerogel synthesis is given in Scheme 1a.

The synthesis of silica sol involves hydrolysis of TEOS ($(OC_2H_5)_3 \equiv Si-OC_2H_5$) by the removal of the ethoxide ($-OC_2H_5$) group and formation of silanol ($(OH)_3 \equiv Si-OH$), as a consequence of the OH^- group reacting with the TEOS precursor, along with the ethoxide group reacting with the H^+ ion, resulting in the formation of ethanol (C_2H_5OH) as a byproduct.

Condensation takes place when particles cause bond formation from the colloidal sol. The formation of sol is favorable when the rate of bond formation is high and the rate of crystal development is low. Inorganic clusters can be colloidal or polymeric in nature, with diameters ranging from 1 to 20 nm depending on the degree of cross-linking and the development procedure used to generate them. The formation of inorganic sols is consistent and stable. The reactions of the "*n*" number of silanol groups condense to generate siloxane linkages, and the byproduct is water molecules.

2.3. Synthesis of Titania-Doped Silica Aerogel. The TdS aerogel is prepared by using a two-step acid–base-catalyzed sol–gel process. In the preparation of 36 mL of sol, solution A was prepared by mixing TEOS, H_2O, EtOH, TTIP, and dil. HCl and magnetically stirred for 12 h at room temperature. The final molar ratio for TdS sol was 1:1.25:9.56:0.011 for TEOS, H_2O, EtOH, and TTIP,

https://doi.org/10.1021/acsomega.3c00552
ACS Omega 2023, 8, 13285–13299

respectively. For the hydrolysis of TEOS, 0.25 mL of 1 N HCl acid was added as a catalyst.

We prepared solution B in the second stage by stirring solution A for 30 min while adding 0.5 mL of a 1 M NH_4F solution. To set the gel, the sol was poured into a quartz mold. The formed sol was then stirred for 1 h, which produced a clear colloidal suspension. The gel was then formed in 24 h and aged in ethanol three times at intervals of 24 h in order to remove water and other solvents from the gel. Furthermore, the gel was dried by the supercritical drying method.

TTIP exhibits similar interactions, with the H^+ ion interacting with the isopropoxide ($-OC_3H_7$) group and the OH^- group binding to the Ti^{4+} species, followed by formation of titanium tetrahydroxide and its byproduct, isopropanol, The use of dil. HCl as an acid catalyst accelerates the rate of the reaction, as demonstrated by the reaction.[29−31] The schematic representation of TdS aerogel synthesis is given in Scheme 1b.

2.4. Characterization Tools. The surface morphology was investigated by field emission scanning electron microscopy (Model JEOL-JSM-6360, Japan) at a 15 kV acceleration voltage and transmission electron microscopy (TEM) analysis using a JEM 2100 Plus (JEOL) at a 200 kV acceleration voltage. A TEM equipped with an energy-dispersive spectroscopy (EDS) detector was utilized to analyze aerogels for the investigation of their surface morphology. To study interatomic bonding interactions between atoms/molecules, the Fourier transform infrared spectrum was observed using an FTIR spectrometer (α Bruker) with scanning from 4000 to 400 cm^{-1}. The material was put on KBr pellets. For thermogravimetric analysis−differential scanning calorimetry (TGA−DSC) analysis, a thermal analyzer from TA Instruments, SDT Q600, was used. The thermal characteristics of aerogels were studied. The aerogel was heated in a N_2 atmosphere at a rate of 10 °C/min from 25 to 1000 °C. The surface area and pore size of the aerogels were characterized by a Brunauer−Emmett−Teller (BET) (NOVA1000e Quantachrome) instrument. X-ray photoelectron spectroscopy (XPS, Model JPS 9030, JEOL ASIA PTE LTD) was used to study the elements, compositions, and chemical bonding in the aerogel.

2.5. Adsorption Experiments. Adsorption experiments were performed at room temperature. The adsorption studies of AC, silica aerogel, and TdS aerogel were performed by mixing the adsorbent (0.1 g) with 20 mL of MB or CV solution while the samples were in the dark. The suspensions were continuously shaken in the dark for 24 h to study the adsorption−desorption equilibrium. To assess the dye concentration, the UV−vis adsorption spectra were acquired using a Cary 60 UV−vis spectrophotometer. Equation 1 was used to calculate the amount of MB and CV dyes adsorbed on AC, silica aerogel, and TdS aerogel.

$$q_t = \frac{(C_0 - C_t)V}{M} \quad (1)$$

where q_t represents the adsorption capacity at time t (mg/g), C_o represents the initial dye concentration (mg/L), C_t represents the dye concentration at time t (mg/L), V (L) represents the initial volume of dye solution, and M (g) represents the amount of the adsorbate.

3. RESULTS AND DISCUSSION

The characterization of the final products (silica and TdS aerogels) is critical for the development of a porous structure and morphology. Various characterization methods such as spectroscopy and electron microscopy were used to investigate the nature, morphology, and composition of aerogels. Aerogel adsorption properties are strongly influenced by their pore volume, surface area, and active sides.

3.1. Morphology Study. Figure S1a−d shows the structural morphology of silica and TdS aerogels, which was studied using field emission scanning electron microscopy (FE-SEM), and it provides substantial information on the porous structure of the material. Aggregation of the aerogel occurs when the spherical-shaped network-like structure of the aerogel grows to a larger size with well-defined boundaries and pores. The pore size varied from 2 to 50 nm, indicating that the material had a mesoporous structure. The high surface-to-volume ratio of these porous structures allows for a large number of active sites, which is perfectly suitable for dye adsorption.

Figure 1a−f shows the TEM images of the as-prepared silica and TdS aerogels using the sol−gel method. It is found that both kinds of aerogels exhibit a mesoporous structure. However, pure silica aerogels (Figure 1a−c) synthesized using TEOS exhibit a bigger pore size than the TdS aerogel (Figure 1d−f) using TEOS/TTIP. On the other hand, by doping titania in the silica aerogel, a relatively low pore volume is observed due to the formation of O−Si−O−Ti−O−Si−O bonding. It can also improve the connectivity between secondary particles. The results of the BET study are consistent with this observation. Due to the gel network's improved ability to endure the differential capillary pressure during the supercritical drying procedure, both aerogels have lower bulk densities and more uniformly distributed pore sizes.[32]

Figure S2a−d describes the elemental mapping of silica aerogels, revealing that they coexist with elements such as Si (Figure S2c) and O (Figure S2d). Furthermore, elemental mapping of TdS aerogels (Figure S2e,f) shows that the elements Si (Figure S2g), O (Figure S2h), and Ti (Figure S2i) are consistently linked along the length of the TdS aerogel. The resulting titania was evenly distributed throughout the surface of the silica aerogel, providing the conformation of the TdS aerogel structure with no additional impurity. In the TEM analysis, a conducting copper grid is applied for aerogel sample deposition. Because the substrate is made of C and Cu, EDS can also identify these elements.

3.2. EDS. The EDS spectrum and the quantitative elemental composition of silica and TdS aerogels are summarized in Figure S3a,b, respectively. The EDS spectrum in Figure S3a gives the confirmation that Si and oxygen are present in the sample of the silica aerogel. Figure S3b illustrates the EDS analysis of the TdS aerogel. Moreover, it is clearly observed that the TdS aerogel is successfully synthesized without any impurity element, and it also verifies that Si, Ti, and O are present. The absorbance peak at 1.75 keV is attributed to the Si atom. The TdS aerogel contains Si, Ti, and O, according to Figure S3b. In the silica aerogel, Si % is 49.52 and O% is 50.48, as shown in Figure S3a. However, the TdS aerogel consists of 47.43% Si, 0.25% Ti, and 52.62% O, as shown in Figure 4b. It is confirmed that titania is successfully doped in the silica

https://doi.org/10.1021/acsomega.3c00552
ACS Omega 2023, 8, 13285−13299

aerogel, according to TEM, EDS, and elemental mapping analysis.

3.3. Fourier Transform Infrared Spectroscopy (FTIR). Figure 2a,b shows an FTIR analysis of silica and TdS aerogels.

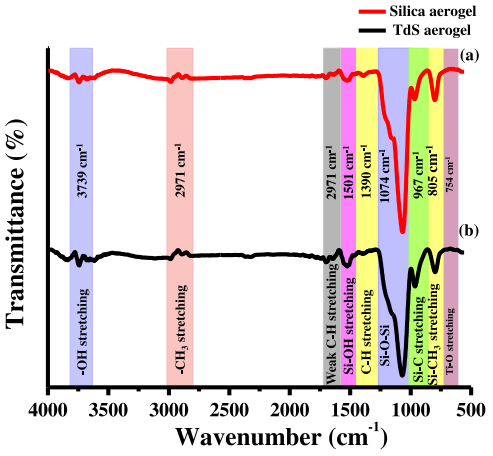

Figure 2. FTIR spectra of (a) silica and (b) TdS aerogels.

The asymmetric stretching and bending vibrations of the Si−O−Si link were responsible for the absorption peaks at 1074 cm^{-1}. It demonstrates that following calcination, the major groups of two aerogels do not alter much. The absorption peaks at roughly 3739 cm^{-1} of the silica aerogel were significantly weaker than those of the TdS aerogel, as shown in Figure 2a,b, because the −OH group on the surface of the aerogel was replaced by the organic group during the modification process. The asymmetric and symmetric vibrations of the $-CH_3$ group emerged at 2971 and 1390 cm^{-1}, respectively, indicating that methyl groups exist on the surface of the silica aerogel. The asymmetric bending and stretching vibration of Si−OH is responsible for the peaks at 967 cm^{-1}. Furthermore, the symmetric stretching vibration of $Si-CH_3$ occurred at 760 cm^{-1}, showing that the $Si-CH_3$ group is present on the surface of the hydrophilic aerogel.[1,4]

3.4. TG−DSC Curve. The TG−DSC graph of the synthesized silica and TdS aerogels is shown in Figure 3a,b. The weight loss was split into two sections in both aerogels. The region of the temperature range 25−300 °C (Section 1) is concerned with the evaporation of water and residual organic solvents. The silica aerogel lost 4.66% of its weight (Section 1), while the TdS aerogel lost 8.6%, resulting in their first exothermic peaks at 175 and 190 °C, respectively. In most cases, this portion is small. Furthermore, because silanol groups bind to the surface hydroxyl groups of silica (silicic acid derivations), the aerogel has a hydrophilic and hygroscopic nature due to the hydroxyl groups on its surface.[33,34] Section 2 explains the weight loss between 350 and 630 °C. The weight loss due to the oxidation of $Si-CH_3$ on the surface of the aerogels results in the second exothermic peak. The second endothermic peak corresponds to the loss at temperatures of 540 and 585 °C, which was responsible for the fast oxidation of $-CH_3$ groups. These observations suggest that both aerogels have the same stability up to a temperature of 630 °C.[35,36] Above 630 °C, no weight loss is observed. It indicates that the aerogels would lose their whole organic sample, leaving just mineral matter at about 1000 °C.

3.5. BET. The N_2 adsorption and desorption isotherms at 77.350 K for silica and TdS aerogels are type IV, with a large hysteresis loop in the ranges of 0.7−0.9 and 0.4−1.0 P/P_0, respectively (Figure 4a,b). The pore size distribution was calculated using the Barrett−Joyner−Halenda (BJH) method, and the corresponding porosity distributions of pure silica and TdS aerogel nanocomposites are shown in Figure S4a,b. The calculated and tabulated porous structural properties for both aerogels are shown in Table 1. Micropores (d less than 2 nm), mesopores (d between 2 and 50 nm), and macropores (d greater than 50 nm) are the three types of pores defined by IUPAC. Silica and TdS, according to our observations, are largely mesoporous. The overall pore volumes of silica and TdS aerogels are 4.162 and 1.337 cm^3/g, respectively. AC has a surface area of 950−2000 m^2/g,[37] whereas synthesized silica and TdS aerogels have 580.504 and 257.579 m^2/g, respectively. The adsorption process may benefit from a mesoporous structural design with a high surface area.[1,38,39]

3.6. XPS. Figure 5a−g shows the XPS analysis of silica and TdS aerogels. The XPS spectra of the silica aerogel in pure form and those of the TdS aerogel were measured for the

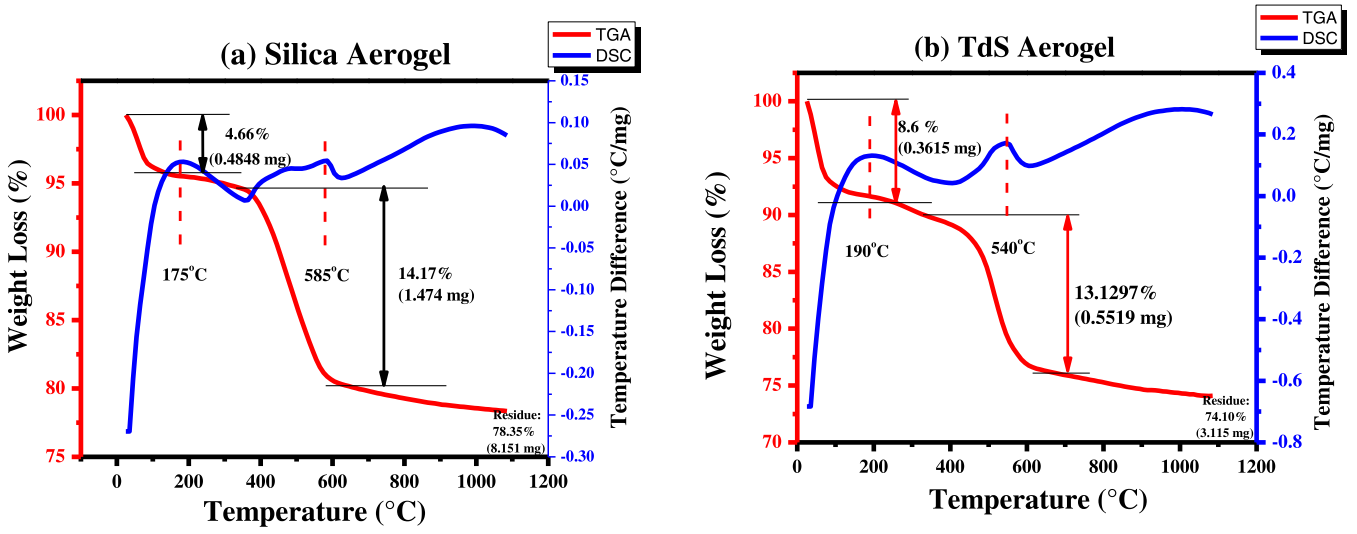

Figure 3. TGA−DSC graph of (a) silica and (b) TdS aerogels.

https://doi.org/10.1021/acsomega.3c00552
ACS Omega 2023, 8, 13285−13299

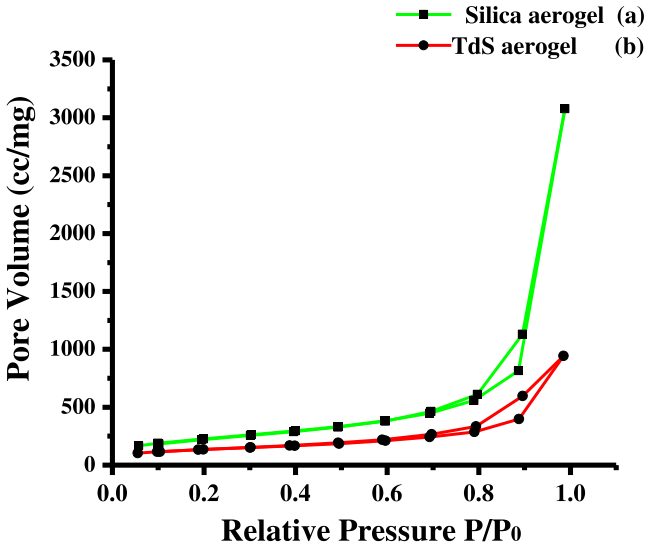

Figure 4. N_2 adsorption and desorption isotherms of the (a) silica and (b) TdS aerogels.

confirmation of titania doping in the silica aerogel. According to their binding energies, the surface scan spectra revealed the existence of Si, Ti, and O atoms. Silica formation is confirmed by Si spectra (Figure 5b,e) observed at 103.46 eV. The configuration of silica is attributed to the $2p_{3/2}$ O−Si−O bond of SiO_4 (tetrahedra). The O 1s peak (Figure 5c,f) can be represented by the silica (O−Si−O) bond, coming from chemical species such as Si−OH and Si−OR.[40] The XPS analysis of a TdS aerogel with a 1.37 atomic wt % titania trace is shown in Figure 5g. The survey spectrum (Figure 5d) confirmed the incorporation of Ti in the silica aerogel. The Ti $2p_{3/2}$ peak (Figure 5g) appeared at 459 eV. The peak value indicates that both Si and Ti were tetravalent.

3.7. Adsorption of Dyes. *3.7.1. Effect of Dye Concentration on Adsorption.* A comparative study of "q_t" is the amount of MB and CV dyes adsorbed (mg/g) with time "t" for various dye concn; the adsorbent dose is 5 g/L AC, silica aerogel, and TdS aerogel.

As the dye concentration increased, the rate of adsorption increased with time. The initial rate of adsorption for AC is faster during the first 90 min, which might be attributed to the surface area. Since the reported surface area of AC is 950−2000 m^2/g[37,41] (avg. surface area is 1475 m^2/g), the surface area values are normalized before comparing with the synthesized aerogel sample. Table 1 shows normalization parameters; first, the AC surface area was normalized with respect to silica and TdS aerogels. Furthermore, because the surface area of the silica aerogel is greater than that of the TdS aerogel, the surface area of the silica aerogel was standardized with respect to the TdS aerogel. However, for silica and TdS aerogels, adsorption increases continuously (but slowly) and reaches equilibrium at 240 min.[42−44]

In the general process of adsorption, the key factor is the impact of pH, which influences the compositions of both dye solutions and adsorbent materials. The parameters of the experiment were not changed. In order to conduct the adsorption experimental studies, 20 mL of an aqueous solution of MB or CV (100 mg/L) was mixed with 0.1 g of AC, silica aerogel, and TdS aerogel. For the point of zero charge (PZC), the silica and TDS aerogel $NaNO_3$ solution was modified utilizing HCl and NaOH solutions to change the pH values between 2 and 11 in order to investigate the impact of pH on the adsorption study. Figure 6 shows the initial color of dye solutions adjusted at each pH ranging from 2 to 11 for the MB and CV dye solutions. Afterward, for 24 h, the solution was kept in a shaking incubator at room temperature with a speed of 300−350 rpm. The maximum absorbance and intensity of the dye's absorption are expected to change as the pH value changes.[1] When the pH falls below 7, the adsorption for MB decreases. A pH of 8 is preferred to be the optimum pH adsorption for MB because when the pH is greater than 8, the circumstance is the opposite, and all % of removal values do not exceed 80%. Because changing the pH caused the CV reduction rate to fluctuate, the maximum pH adsorption value for CV was thought to be 7.[45] Because the reduction rate of CV varied with pH, a pH of 7 was considered to be the optimal pH adsorption for CV. This analysis found that silica and TdS aerogels had a point of zero charge (PZC) of 2.02. Negative charges can self-assemble on the adsorbent's surface, and when the adsorbent material was combined with the dyes that contained positive charges, it was conducive to the adsorption process. As a result, cationic dyes are effectively absorbed by AC, silica aerogel, and TdS aerogel, when the pH of the solution is higher than that of the point at which silica has no charge.

3.7.2. Initial Dye Concentration Impact. While maintaining the control parameters, the preliminary dye concentration of the adsorption process is studied. The adsorption rate decreases with MB and CV concentration. The highest amount of dye adsorbed (the "q_t" value vs time) by AC, silica aerogel, and TdS aerogel for the MB dye is 97.26, 61.19, and 128.71 mg/g, respectively. Furthermore, using the same adsorbents, the adsorption of CV dye was 94.83, 61.15, and 114.50 mg/g, respectively (shown in Figures 7 and S5).

3.7.3. Study of Adsorption Isotherms. In the adsorption, compound concentration (mg/L) and the compound concentration remaining on solid particles q (mg/g) can be investigated. The equation $q = f(C)$ gives rise to the sorption

Table 1. Pore Size Distribution of Silica and TdS Aerogel Samples[a]

aerogel samples	pore volume (cm^3/g)	surface area (m^2/g)	average pore radius (nm)	normalization factors for the surface area of silica and TdS aerogels with respect to activated charcoal	normalization factor for the surface area of TdS with respect to silica aerogel
activated charcoal	0.201[b]	1475 avg. (reported range 950−2000)[b]	2.669[b]		
silica	4.612	580.504	26.7064	$\frac{1475}{580.504} = 2.541$	
TdS	1.337	257.579	17.9470	$\frac{1475}{257.579} = 5.726$	$\frac{580.504}{257.579} = 2.25$

[a]The AC surface area was normalized with respect to silica and TdS aerogels. Furthermore, the surface area of the silica aerogel was normalized with respect to the TdS aerogel. [b]Values taken from refs 37, 41.

https://doi.org/10.1021/acsomega.3c00552
ACS Omega 2023, 8, 13285−13299

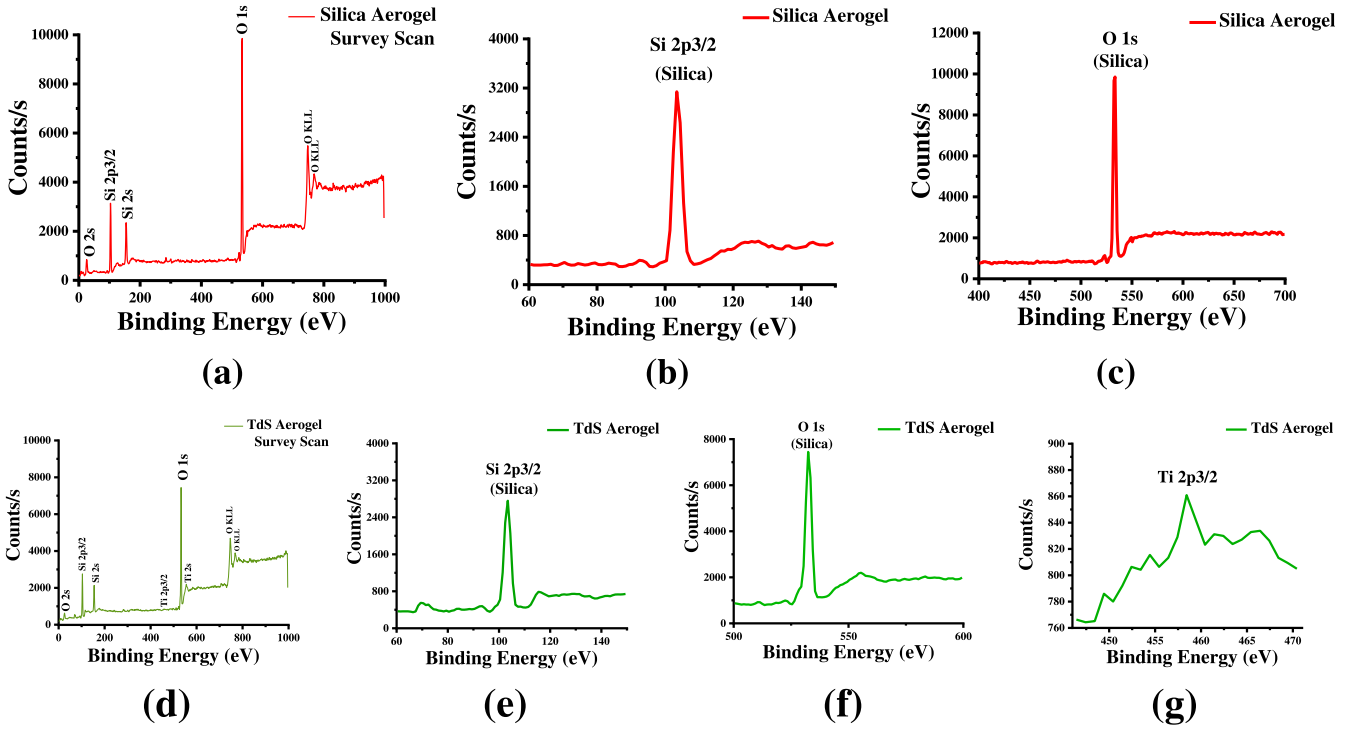

Figure 5. XPS of the (a–c) silica and (d–g) TdS aerogels.

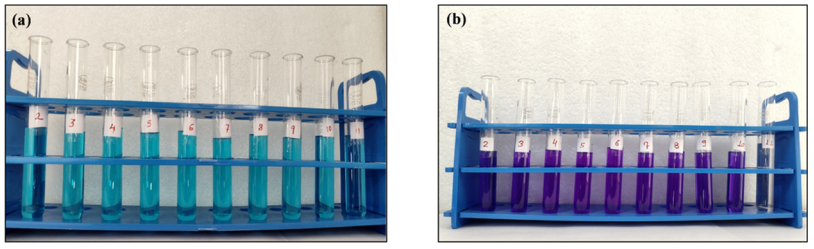

Figure 6. Initial images of dye solutions adjusted at each pH ranging from 2 to 11: (a) MB dye solution and (b) CV dye solution.

isotherm. Due to the uniqueness of this correlation, several requirements must be met: (I) all adsorption/desorption equilibria must be accomplished, and (II) all other physical and chemical parameters must remain unchanged. Because temperature is very important in sorption processes, the term "isotherm" was particularly adopted (temperature must be constant and specified).[46] Sorption isotherms were classified by Giles et al.[47] Based on their initial slopes and curvatures, they classified constant partition (*C*), Langmuir (*L*), high affinity (*H*), and sigmoidal-shaped (*S*) isotherm classes.[48] The adsorption isotherm describes the connection between the amount of the adsorbate and the adsorbent surface. Adsorption equilibrium is reached if the adsorbate and adsorbent have been in contact for a sufficient time.[42−44] Langmuir isotherms (Figures 8 and 9) were used to analyze adsorption equilibrium.

3.7.3.1. Langmuir Adsorption Isotherms. In the earlier days, the Langmuir adsorption isotherm, which was first established to classify gas−solid phase adsorption onto activated charcoal, has been employed to assess and compare the effectiveness of various biosorbents. This experimental approach is based on the assumption that adsorption occurs in a monolayer, i.e., the adsorbed layer is one molecule thick, that adsorption can only take place at a predefined (fixed) total count of sites on the surface that are similar and comparable, and that there is no lateral interaction or steric hindrance between adsorbate species, even on adjacent sites. There is also no reincarnation of the adsorbate on the plane surface. The Langmuir isotherms explain relatively homogeneous adsorption, where each of the molecules has equality for both the adsorbate and constant enthalpies and sorption activation energies. There can be no further sorption at a surface site after it has been filled. As a result, the surface will ultimately approach a saturation point, at which its maximum adsorption will be accomplished.[42] The Langmuir isotherm model equation's nonlinear form is as follows:

$$\frac{C_e}{q_e} = \frac{1}{K_L Q_{max}} + \frac{C_e}{Q_{max}} \quad (2)$$

where q_e (mg/g) is the amount of dye adsorbed at equilibrium, Q_{max} (mg/g) is the maximum adsorption capacity of the absorbents, and K_L is constant for Langmuir adsorption. To determine exactly whether the adsorption is beneficial, the equilibrium parameter R_L is used. It can be explained by the following equation:

$$R_L = \frac{1}{1 + K_L C_o} \quad (3)$$

https://doi.org/10.1021/acsomega.3c00552
ACS Omega 2023, 8, 13285−13299

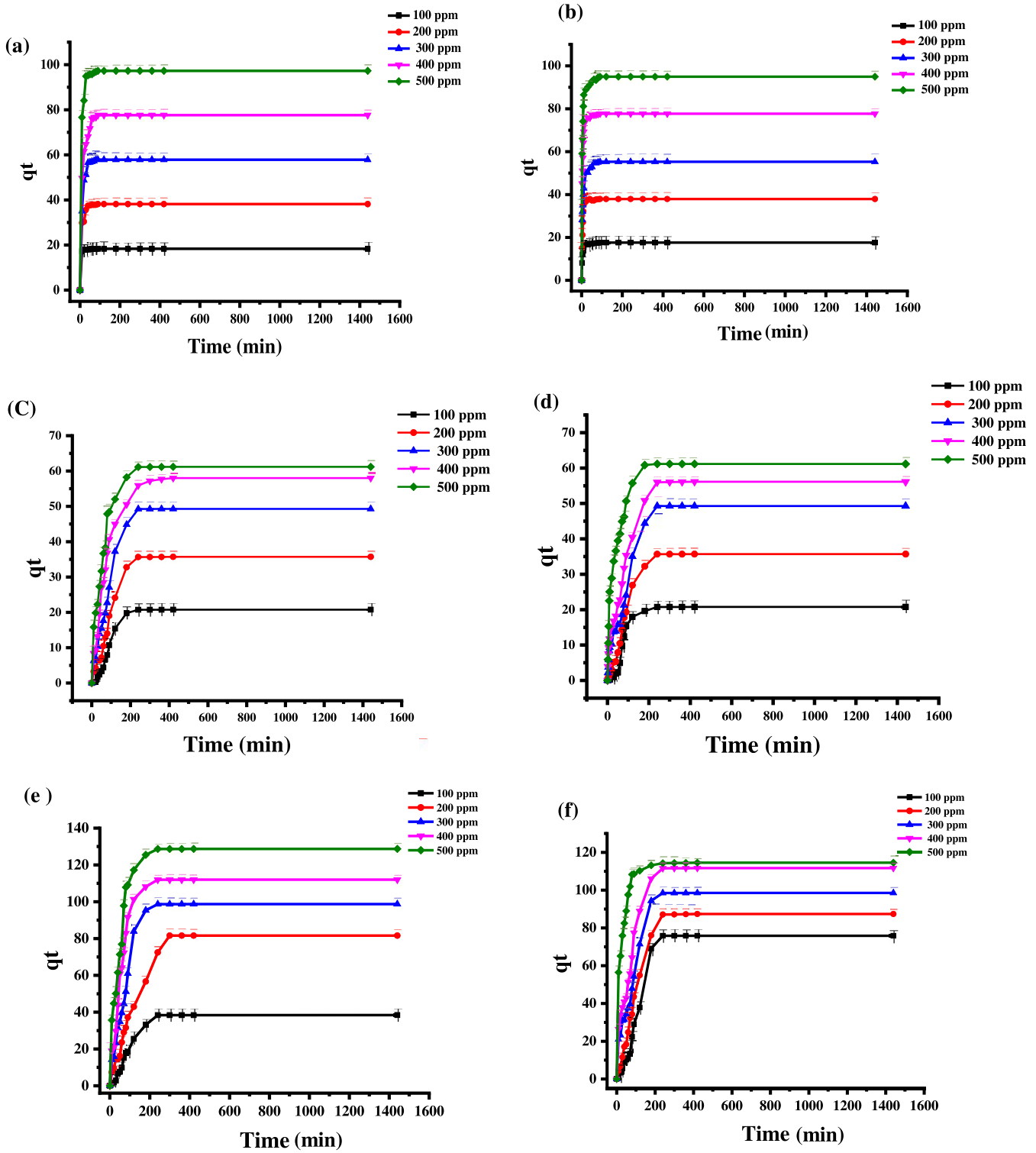

Figure 7. Plot of adsorption at time t (q_t) against incubation time for (a) MB on AC, (b) CV on AC, (c) MB on the silica aerogel (q_t normalized to the surface area of AC), (d) CV on the silica aerogel (q_t normalized to the surface area of AC), (e) MB on the TdS aerogel (q_t normalized to the surface area of AC), and (f) CV on the TdS aerogel (q_t normalized to the surface area of AC).

where C_o (mg/g) denotes the initial concentration of the dye, and K_L (L/g) denotes the constant of Langmuir isotherm adsorption. If the values of R_L are between 0 and 1, then the process of adsorption is considered successful, and if the values are greater than 1, then the adsorption process is not favorable.[49] If the formula could adequately express the adsorption process, then the procedure is single-molecule layer adsorption.[50]

The nonlinear plot of q_e versus C_e shows the applicability of the Langmuir isotherm model, as given in Figures 8 and 9. The Langmuir isotherm suggests the monolayer coverage of MB and CV on AC, silica aerogel, and TdS aerogel. The comparative study (shown in Tables 2 and 3) of AC, silica

https://doi.org/10.1021/acsomega.3c00552
ACS Omega 2023, 8, 13285−13299

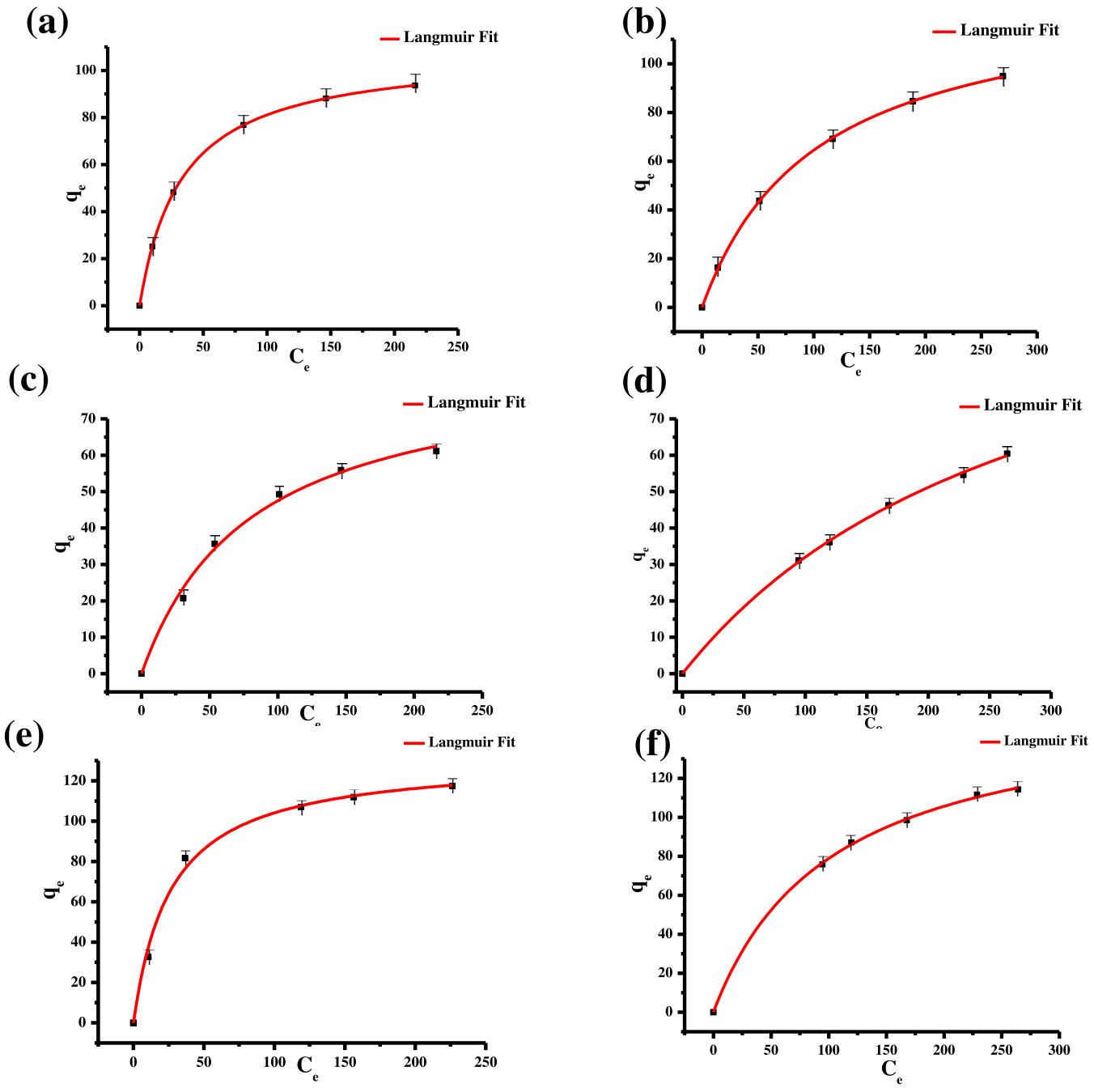

Figure 8. Adsorption isotherms of adsorbed onto (a) MB on AC, (b) CV on AC, (c) MB on the silica aerogel (q_e normalized to the surface area of AC), (d) CV on the silica aerogel (q_e normalized to the surface area of AC), (e) MB on the TdS aerogel (q_e normalized to the surface area of AC), and (f) CV on the TdS aerogel (q_e normalized to the surface area of AC).

aerogel, and TdS aerogel reveals that the TdS aerogel has a greater Q_{max} value for MB and CV dyes. The Q_{max} value of TdS increases 1.22 times compared to AC and 1.25−1.53 times compared to the silica aerogel. In the case of silica, the Q_{max} value decreases 1.08−1.26 times compared to AC. The chi-square value denotes the difference between the observed and expected values. Thus, the Langmuir isotherm fits minimum chi-square values compared to other isotherms. Therefore, the adsorption isotherm on the newly synthesized silica aerogel, TdS, shows the Langmuir isotherm.

3.7.3.2. Freundlich Adsorption Isotherm. The previously known correlation that describes nonideal and reversible adsorption, not just the establishment of monolayers, is said to be the Freundlich isotherm. This quantitative model is applicable to multilayer adsorption with nonuniform adsorption at high temperatures and affinity dispersion over the heterogeneous surface. This was originally created to demonstrate that the proportion of the adsorbate to the solute on a provided mass of the adsorbent was not consistent at different solution concentrations.[51,52] According to this viewpoint, the quantity adsorption is the total amount that has been adsorbed on all of the sites (each of which has bond energy), with the more powerful active sites being filled initially until the portion of adsorption energy has tremendously reduced after the procedure is complete. Freundlich's equation is written as follows in the nonlinear form:

https://doi.org/10.1021/acsomega.3c00552
ACS Omega 2023, 8, 13285−13299

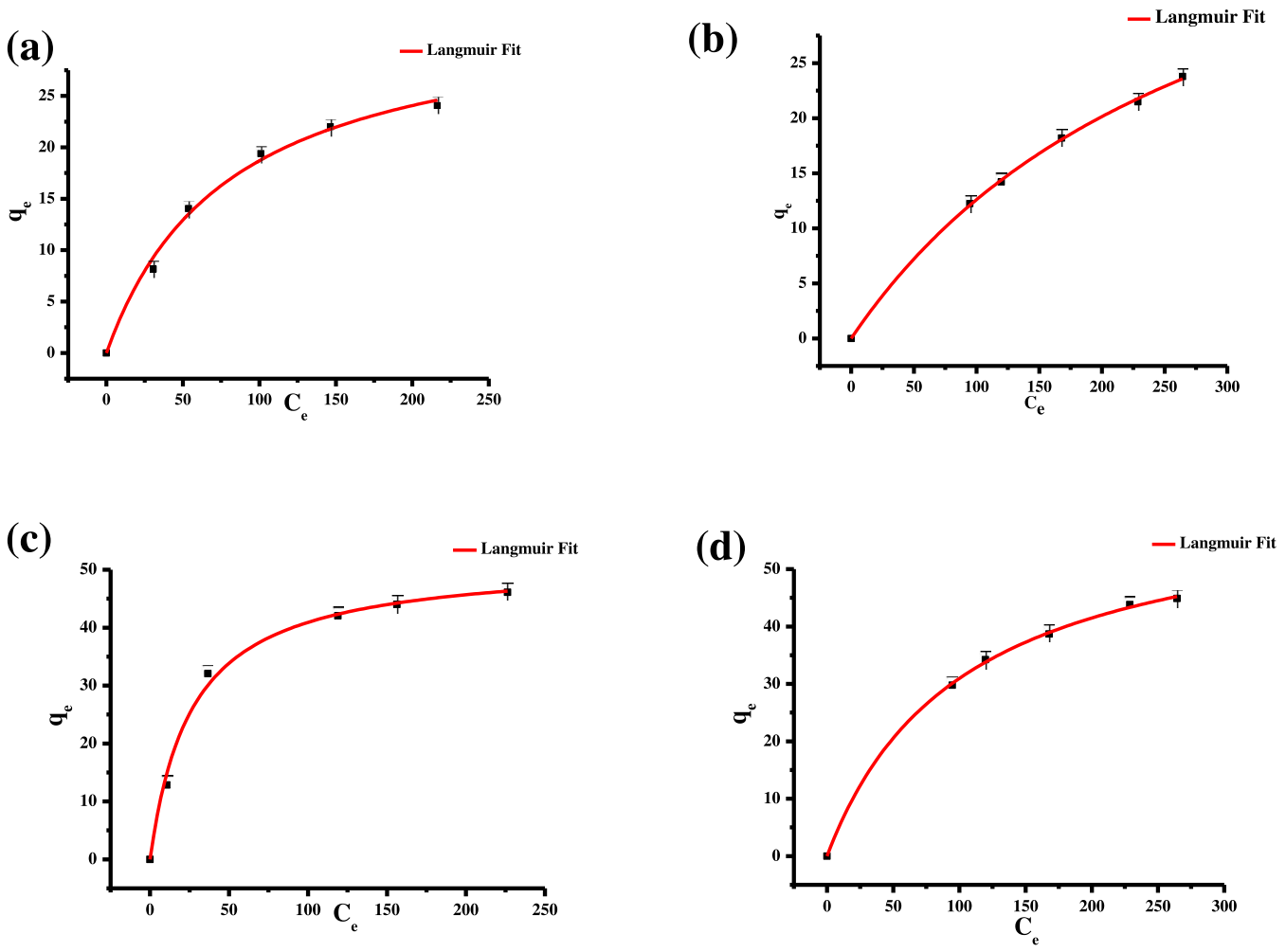

Figure 9. Adsorption isotherms of adsorbed onto (a) MB on the silica aerogel, (b) CV on the silica aerogel, (c) MB on the TdS aerogel (q_e normalized to the surface area of the silica aerogel), and (d) CV on the TdS aerogel (q_e normalized to the surface area of the silica aerogel).

Table 2. Adsorption of Dyes by Adsorbents AC, Silica Aerogel, and TdS Aerogel Obtained from the Langmuir, Freundlich, and Temkin Isotherm Models[a]

		MB			CV		
adsorption isotherms		AC	silica	TdS	AC	silica	TdS
Langmuir	R^2	0.9999	0.99933	0.99447	0.9991	0.99333	0.99935
	Q_{max} (mg/g)	108.0382	85.7340	131.5877	130.503	50.1283	159.889
	K_L (L/mg)	0.03	0.01244	0.03792	0.00977	0.00336	0.00972
	chi-square	0.02025	0.63659	12.89256	0.1259	0.0486	1.1624
Freundlich	R^2	0.97356	0.97124	0.95405	0.9689	0.9992	0.9978
	K_F (mg/g)	14.0368	5.3254	21.7385	5.79099	0.67506	13.3505
	$1/n$	2.75319	0.4639	0.2905	1.97338	0.6388	0.4972
	n	0.36321	2.1554	3.10349	0.50674	1.5659	2.55771
	chi-square	37.106	15.6805	107.063	4.36896	0.05776	3.8534
Temkin	R^2	0.9689	0.99371	0.98428	0.98377	0.9884	0.9990
	Q_{max} (mg/g)	22.9469	20.7851	61.669	26.925	28.4158	37.6300
	K_t (L/mg)	0.30599	0.09703	0.3852	0.1171	0.03063	0.08168
	chi-square	4.36896	3.42671	36.6242	9.01968	0.11587	1.7135

[a] q_e normalize with AC.

$$q_e = K_F C^{1/n} \quad (4)$$

The amount of adsorbed dye on the adsorbent is denoted q_e (mg/g), and the approximate capacity of adsorption is denoted K_F. Chemical adsorption occurs when $1/n < 1$, whereas physical adsorption is more preferred when $1 < 1/n < 10$.[53,54] The Freundlich isotherm is currently used as extensively throughout distributed, i.e., heterogeneous systems, particularly for organic compounds or highly dynamic species on adsorbents and activated charcoal. In contrast, an amount

https://doi.org/10.1021/acsomega.3c00552
ACS Omega 2023, 8, 13285−13299

Table 3. Adsorption of Dyes by the Adsorbents Silica and TdS Aerogels Obtained from the Langmuir, Freundlich, and Temkin Isotherm Models[a]

		MB		CV	
adsorption isotherms		silica	TdS	silica	TdS
Langmuir	R^2	0.99933	0.99447	0.99333	0.99935
	Q_{max} (mg/g)	33.7402	51.7066	50.1283	62.8277
	K_L (L/mg)	0.01244	0.03792	0.00336	0.00972
	chi-square	0.5632	1.9906	0.0486	0.1795
Freundlich	R^2	0.97124	0.9540	0.9992	0.9978
	K_F (mg/g)	2.0958	8.54206	0.67506	5.2460
	$1/n$	0.4639	0.2905	0.6388	0.4972
	n	2.1554	3.10349	1.5659	2.55771
	chi-square	15.6805	16.5311	0.05776	0.5949
Temkin	R^2	0.99371	0.96428	0.9984	0.9990
	Q_{max} (mg/g)	20.7851	10.7696	11.1829	14.786
	K_t (L/mg)	0.09703	0.3852	0.03063	0.08168
	chi-square	3.42671	5.6549	0.1158	0.2645

[a] q_e normalize with the silica aerogel.

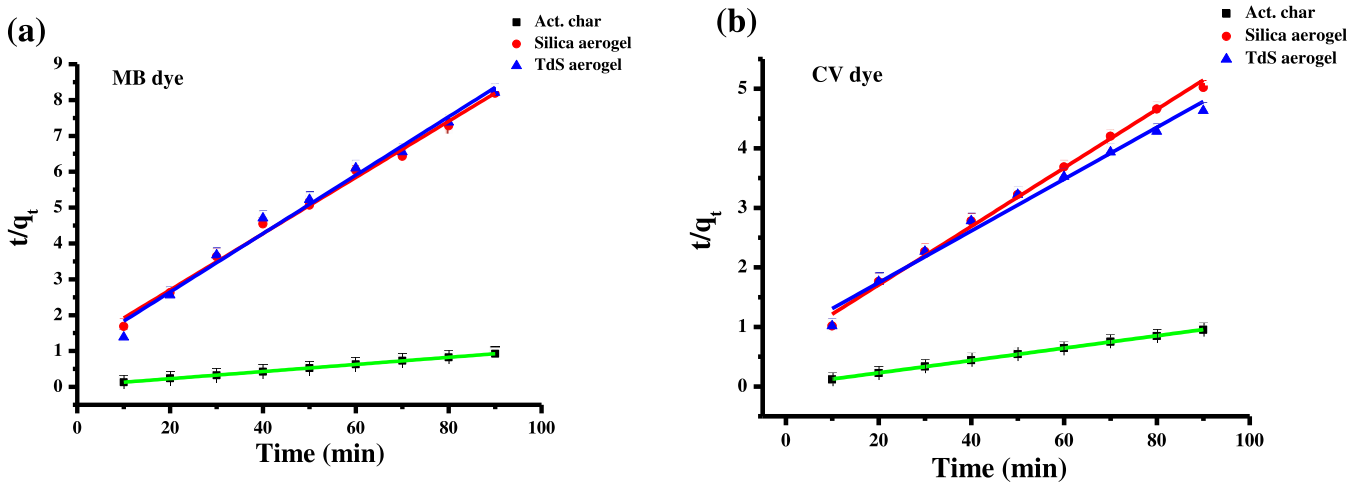

Figure 10. Kinetic models for the adsorption of (a) methylene blue onto AC, silica aerogel, and TdS aerogel and (b) crystal violet dyes onto AC, silica aerogel, and TdS aerogel for pseudo-second-order kinetics.

lower than 1 denotes chemisorption, and $1/n$ greater than 1 denotes physisorption.

3.7.3.3. Temkin Adsorption Isotherm. A founding approach that was used to examine hydrogen adsorption on platinum electrodes in acid solutions was the Temkin isotherm. Adsorbent−adsorbate connections are clearly taken into consideration by a component in the kinetic model. The method makes the assumption that perhaps the heat of adsorption (a function of temperature) among all substances inside the surface might well reduce linearly rather than logarithmically with scope by disregarding the exceptionally both low and high concentration values. Its mathematical formalism is indicated by an even distribution of binding energies (up to the highest binding energy), as indicated by an equation.

Temkin's equation is often unsuitable for modeling complex adsorption systems, including liquid-phase adsorption isotherms (where organization in a densely packed structure with a similar orientation is not required). The constants were found by graphing the amount of adsorbed Q_e versus C_e and determining Q_m and K_T, as specified in the equation. The equation that describes the model is as follows:

$$q_e = Q_m \ln(K_T C_e) \quad (5)$$

The Temkin isotherm constant is related to the heat of sorption "Q_m" (RT/b_T; J/mol), R is the universal gas constant [8.314 J/(mol K)], T is the temperature at 298 K, and K_T represents the Temkin isotherm equilibrium binding constant (L/g), "q_e" is the amount of adsorbate adsorbed (mg/g), "C_e" is the adsorbate equilibrium concentration (mg/dm^3).

In Figures S6 and S7, we show the Langmuir, Freundlich, and Temkin isotherm fitting experimental data. The higher regression coefficient R^2 values and lower chi-square value indicate that the Langmuir isotherm is most appropriate for the adsorption of AC, silica aerogel, and TdS aerogel.

3.7.4. Kinetic Models. The use of suitable kinetic models can provide insights into the mechanisms of fundamental adsorption. The most frequently used equations are those for second-order models. For second-order models, the kinetic parameters of the adsorption of both MB and CV dyes by AC, silica aerogel, and TdS aerogel are investigated. The general expression for the second-order linear system is as follows:

$$\frac{t}{q_t} = \frac{1}{k_2 Q_e^{\ 2}} + \frac{t}{q_e} \quad (6)$$

https://doi.org/10.1021/acsomega.3c00552
ACS Omega 2023, 8, 13285−13299

Table 4. Pseudo-Second-Order Parameters for Dye Adsorption by Adsorbents AC, Silica Aerogel, and TdS Aerogel

dyes	adsorbents	Q_e, c (mg/g)	k_2 (g/mg·min)	R^2	R_L	chi-square
MB	AC	100	0.322307	0.99962	0.25094	0.0002
	silica	12.6742	0.000141	0.99231	0.44563	0.0001
	TdS	12.3456	0.00015	0.98386	0.20868	0.0003
CV	AC	96.24639	0.50564	0.9997	0.50581	0.00012
	silica	20.3541	0.000575	0.99414	0.74850	0.00031
	TdS	22.99379	0.006078	0.9619	0.50709	0.00023

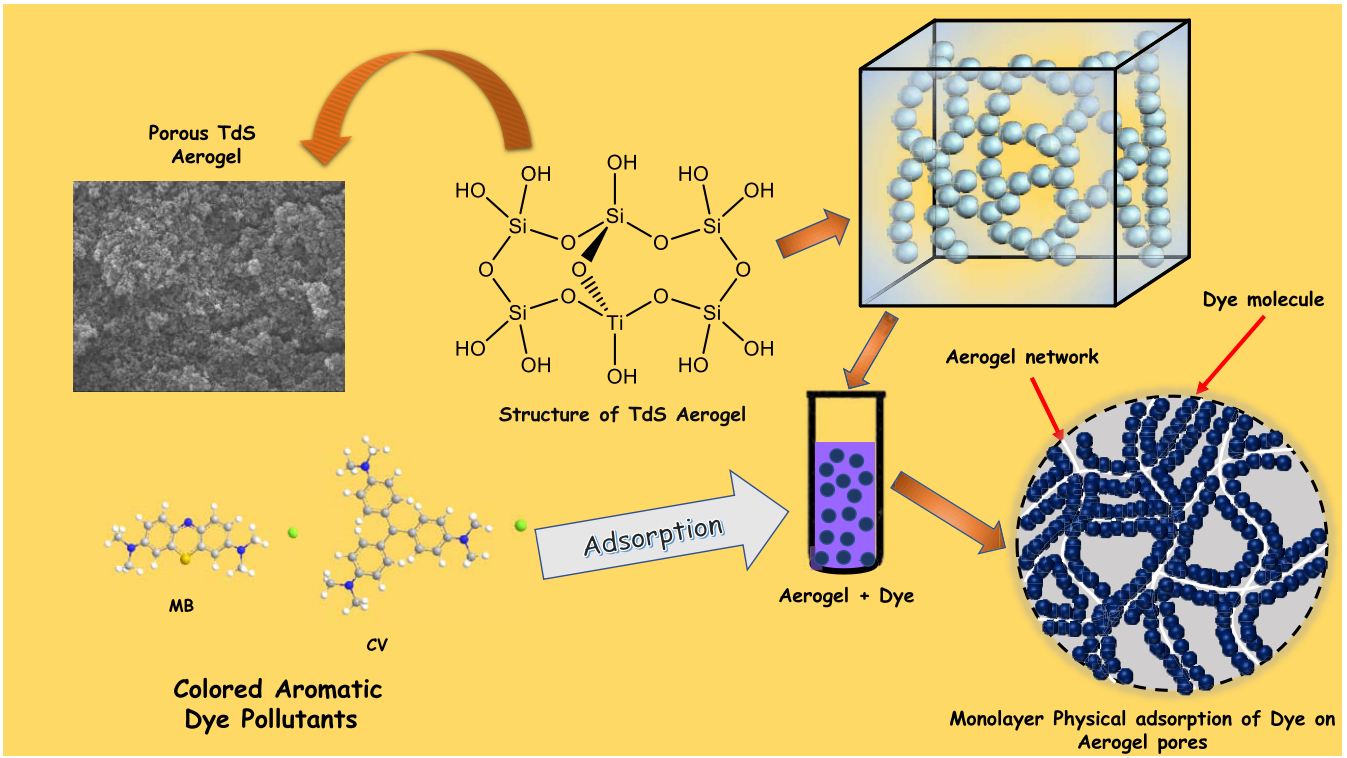

Figure 11. Schematic representation of physical adsorption of the dye on the surface of the TdS aerogel.

The number of adsorption potentials at equilibrium and time t (h), respectively, are denoted by q_e (mg/g) and q_t (mg/g). The second-rate constant ($1/h$) is known as k_2, as depicted in Figure 10.

However, the behavior across the entire adsorption distance seems to be predicted by the pseudo-second-order model. The coefficients of correlation ($R_{AC\text{-}MB}^2$ = 0.99892, $R_{silica\text{-}MB}^2$ = 0.98654, $R_{TdS\text{-}MB}^2$ = 0.98386, $R_{AC\text{-}CV}^2$ = 0.99956, $R_{silica\text{-}CV}^2$ = 0.98027, and $R_{TdS\text{-}CV}^2$ = 0.98192) were just about nearly constant. The determined Q_e (cal) was approximately consistent with Q_e (exp) (Q_{AC} = 100, $Q_{silica\text{-}MB}$ = 12.41619071, $Q_{TdS\text{-}MB}$ = 40.65, $Q_{AC\text{-}CV}$ = 95.33, $Q_{silica\text{-}CV}$ = 18.86, $Q_{TdS\text{-}CV}$ = 23.25 mg/g). The research findings in Table 4 thus revealed that the pseudo-second-order mechanism can provide a clearer explanation of the adsorption kinetics for the adsorption of MB and CV dyes.[55]

3.7.5. Adsorption Mechanism. Depending on the diverse ways that the adsorbent and adsorbate converse, physical adsorption and chemical adsorption can be distinguished from one another in the classical physical chemistry principle of adsorption. The van der Waals (vdW) forces between the adsorbent and the adsorbate are the primary connections for physical adsorption. The adsorption mechanism is physical adsorption because there are no chemical bonds created between the adsorbents (silica and TdS aerogel) and cationic dyes (MB and CV). Figure 11 shows the schematic representation of the physical adsorption of the dye on the surface of the adsorbate (i.e., silica and TdS aerogels).

The principal factors that impacted the physical adsorption process included the electrostatic effect and the steric hindrance intensity of the adsorbate. When the theoretical model test results were compared to the adsorption capacity, it was found that silica and TdS had better adsorption capacities for MB than those for CV; similar results by experimental calculations were obtained. From the resulting adsorption findings, silica and TdS have a lot of hydroxyl (−OH) groups on their surface, which adsorb on the adsorbate by electrostatic interaction among them. Despite having a small spatial capacity, CV has difficulty forming a hydrogen bond with the adsorbent. The majority of the dye molecules' negative ions are concentrated around their carbon and sulfur atoms, and both dyes have almost similar negative charges.[56] As a result, the electrostatic effect makes it simpler for MB and CV with such a higher density of positive ions to bind to the aerogel with negative ions. Since there are no electronic donors or receptors on the molecules in the MB and CV solutions, vdW is primarily responsible for the adsorption impact.

3.7.6. Regeneration of Saturated Adsorbents. To design a cutting-edge and effective adsorbent, reuse and repeatability are very crucial and critical factors. A useful adsorbent should

https://doi.org/10.1021/acsomega.3c00552
ACS Omega 2023, 8, 13285−13299

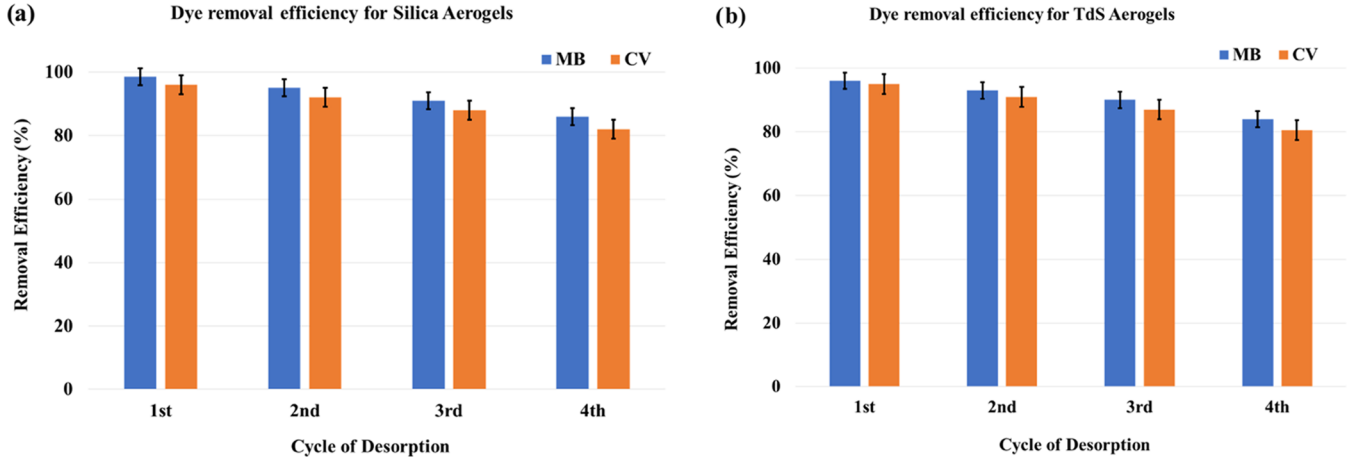

Figure 12. Removal efficiency of MB and CV onto (a) silica and (b) TdS aerogels in four cycles.

Table 5. Compares MB and CV Dyes' Maximum Adsorption Capacities (Q_{max}) for Silica and TDS Aerogels with Those of Other Reported Adsorbent Materials

adsorbent	max. adsorption capacity (Q_{max}) (mg/g)	pH	dye concentration (mg/L)	reference
hydrophobic silica aerogel	65.74	7.0	500 (MB)	1
lignin-based activated carbon	600	5.2	4.4 (CV)	57
resorcinol-formaldehyde-activated carbon xerogel	121.53	7.0	150 (CV)	58
sugarcane leaf-activated charcoal	149.25	9.0	100 (CV)	59
activated charcoal	108.0382	8.0	500 (MB)	present work
	131.5877	7.0	500 (CV)	
silica aerogel	85.73	8.0	500 (MB)	
	50.12	7.0	500 (CV)	
TdS aerogel	131.58	8.0	500 (MB)	
	159.89	7.0	500 (CV)	

possess a greater capacity for adsorption as well as increased desorption effectiveness, which will lower the adsorbent's expense. The silica and TdS aerogels were thoroughly cleaned with ethanol to allow the dye to be released after adsorption in order to reveal the cycle test. It can be seen in Figure 12 that by the completion of four cycles of adsorption, both dyes' adsorption efficiency was around 86%. According to the evidence, silica and TDS aerogels were indeed sustainable adsorbents for MB and CV dyes.The TdS adsorption rate slightly decreases after the third cycle, as shown in Figure 12b, and after the fourth cycles, we get 84 and 80% for MB and CV dyes, respectively. Its outcome also showed that silica/TdS can be utilized as an effective adsorption method multiple times for the treatment of dye wastewater.

Table 5 compares MB and CV dyes' maximum adsorption capacities (Q_{max}) for silica and TDS aerogels with those of other reported adsorbent materials. Thus, the newly synthesized TdS aerogel is found to be durable, reusable, and recoverable. The TdS aerogel efficiently removes the dyes from an aqueous solution with potential application in wastewater treatment.

4. CONCLUSIONS

The newly synthesized TdS aerogel was compared to the silica aerogel and AC for the removal of azo dyes (MB and CV) by adsorption. The TdS and silica aerogels are characterized to exhibit mesoporous structures with an average pore radius of 1.80−48 nm. The surface areas of silica and TdS aerogels are 580.504 and 257.579 m^2/g, respectively, which are lesser than that of activated charcoal (average value of 1475 m^2/g)[37,40] and hence are normalized to activated charcoal for further investigation. The comparative study of AC, silica aerogel, and TdS aerogel reveals that the TdS aerogel has a greater Q_{max} value for MB and CV dyes. The Q_{max} value of TdS increases 1.22 times compared to AC and 1.25−1.53 times compared to the silica aerogel. In the case of silica, the Q_{max} value decreases 1.08−1.26 times compared to AC. Furthermore, the adsorption process follows a pseudo-second-order kinetic reaction rate. Both the silica and TdS aerogels' experimental data are well suited to the Langmuir isotherms, which represent a physisorption and monolayer adsorption isotherm. Thus, the newly synthesized TdS aerogel is found to be durable, reusable, and recoverable. The TdS aerogel efficiently removes the dyes from aqueous solutions with potential application in wastewater treatment.

■ ASSOCIATED CONTENT

Supporting Information

The Supporting Information is available free of charge at https://pubs.acs.org/doi/10.1021/acsomega.3c00552.

Morphology study; EDS; BET; initial dye concentration impact; adsorption study; morphology study; and Figures S1−S9 (PDF)

■ AUTHOR INFORMATION

Corresponding Author

Kiran Kumar K. Sharma − *School of Nanoscience and Biotechnology, Shivaji University, Kolhapur 416004*

https://doi.org/10.1021/acsomega.3c00552
ACS Omega 2023, 8, 13285−13299

Maharashtra, India; orcid.org/0000-0003-1823-1934; Email: kks.snst@unishivaji.ac.in

Authors

Prashant D. Sarvalkar − *School of Nanoscience and Biotechnology, Shivaji University, Kolhapur 416004 Maharashtra, India;* orcid.org/0000-0001-6768-6797

Apurva S. Vadanagekar − *School of Nanoscience and Biotechnology, Shivaji University, Kolhapur 416004 Maharashtra, India*

Omkar S. Karvekar − *School of Nanoscience and Biotechnology, Shivaji University, Kolhapur 416004 Maharashtra, India*

Pramod D. Kumbhar − *Department of Chemistry, Shivaji University, Kolhapur 416004 Maharashtra, India; Department of Chemistry, Sadguru Gadge Maharaj College, Karad 415124 Maharashtra, India*

Santosh S. Terdale − *Department of Chemistry, Savitribai Phule Pune University, Pune 411007 Maharashtra, India*

Avinash Singh Thounaojam − *Department of Chemistry, AKI's Poona College of Arts, Science & Commerce, Pune 411001 Maharashtra, India*

Sanjay S. Kolekar − *Department of Chemistry, Shivaji University, Kolhapur 416004 Maharashtra, India*

Rajiv S. Vhatkar − *Department of Physics, Shivaji University, Kolhapur 416004 Maharashtra, India;* orcid.org/0000-0003-2332-1571

Pramod S. Patil − *School of Nanoscience and Biotechnology, Shivaji University, Kolhapur 416004 Maharashtra, India; Department of Physics, Shivaji University, Kolhapur 416004 Maharashtra, India*

Complete contact information is available at: https://pubs.acs.org/10.1021/acsomega.3c00552

Notes

The authors declare no competing financial interest.

■ ACKNOWLEDGMENTS

The authors acknowledge DST supported "Sophisticated Analytical Instrument Facilities (SAIF) in Shivaji University, Kolhapur, Maharashtra" for providing with "FTIR, TEM, XPS" facility accessed through I-STEM (Indian Science, Technology, and Engineering facilities Map) portal, supported by the office of the Principal Scientific Adviser to the Govt. of India. The author P.D.S. is thankful to the Chhatrapati Shahu Maharaj National Research Fellowship (CSMNRF-2021) from the Government of Maharashtra, India, for financial support. K.K.K.K.S. acknowledges funding from RUSA under Centre for Nanofabrics.

■ REFERENCES

(1) Han, H.; Wei, W.; Jiang, Z.; Lu, J.; Zhu, J.; Xie, J. Removal of Cationic Dyes from Aqueous Solution by Adsorption onto Hydrophobic/Hydrophilic Silica Aerogel. *Colloids Surf., A* **2016**, *509*, 539−549.

(2) Xu, H.; Zhu, P.; Wang, L.; Jiang, Z.; Zhao, S. Structural Characteristics and Photocatalytic Activity of Ambient Pressure Dried SiO2/TiO2 Aerogel Composites by One-Step Solvent Exchange/Surface Modification. *J. Wuhan Univ. Technol., Mater. Sci. Ed.* **2016**, *31*, 80−86.

(3) Wan, J.; Xu, L. H.; Pan, H.; Wang, L. M.; Shen, Y. Green Water-Based Fabrication of SiO2−TiO2 Aerogels with Superhydrophobic and Photocatalytic Properties and Their Application on Cotton Fabric. *J. Porous Mater.* **2021**, *28*, 1501−1510.

(4) Biradar, A. I.; Sarvalkar, P. D.; Teli, S. B.; Pawar, C. A.; Patil, P. S.; Prasad, N. R. Photocatalytic Degradation of Dyes Using One-Step Synthesized Silica Nanoparticles. *Mater. Today Proc.* **2021**, *43*, 2832−2838.

(5) Sarvalkar, P. D.; Mandavkar, R. R.; Nimbalkar, M. S.; Sharma, K. K.; Patil, P. S.; Kamble, G. S.; Prasad, N. R. Bio-Mimetic Synthesis of Catalytically Active Nano-Silver Using Bos Taurus (A-2) Urine. *Sci. Rep.* **2021**, *11*, No. 16934.

(6) Gadekar, M. R.; Ahammed, M. M. Coagulation/Flocculation Process for Dye Removal Using Water Treatment Residuals: Modelling through Artificial Neural Networks. *Desalin. Water Treat.* **2016**, *57*, 26392−26400.

(7) da Silva, L. F.; Barbosa, A. D.; de Paula, H. M.; Romualdo, L. L.; Andrade, L. S. Treatment of Paint Manufacturing Wastewater by Coagulation/Electrochemical Methods: Proposals for Disposal and/or Reuse of Treated Water. *Water Res.* **2016**, *101*, 467−475.

(8) Sharma, S.; Malaviya, P. Bioremediation of Tannery Wastewater by Chromium Resistant Novel Fungal Consortium. *Ecol. Eng.* **2016**, *91*, 419−425.

(9) Naushad, M.; Khan, M. R.; ALOthman, Z. A.; Awual, M. R. Bromate Removal from Water Samples Using Strongly Basic Anion Exchange Resin Amberlite IRA-400: Kinetics, Isotherms and Thermodynamic Studies. *Desalin. Water Treat.* **2016**, *57*, 5781−5788.

(10) Rezvani-Boroujeni, A.; Javanbakht, M.; Karimi, M.; Shahrjerdi, C.; Akbari-adergani, B. Immoblization of Thiol-Functionalized Nanosilica on the Surface of Poly(Ether Sulfone) Membranes for the Removal of Heavy-Metal Ions from Industrial Wastewater Samples. *Ind. Eng. Chem. Res.* **2015**, *54*, 502−513.

(11) Feng, Z.; Zhu, S.; Martins de Godoi, D. R.; Samia, A. C. S.; Scherson, D. Adsorption of Cd2+on Carboxyl-Terminated Superparamagnetic Iron Oxide Nanoparticles. *Anal. Chem.* **2012**, *84*, 3764−3770.

(12) Kharisov, B. I.; Rasika Dias, H. V.; Kharissova, O. V.; Manuel Jiménez-Pérez, V.; Olvera Pérez, B.; Muñoz Flores, B. Iron-Containing Nanomaterials: Synthesis, Properties, and Environmental Applications. *RSC Adv.* **2012**, *2*, 9325.

(13) Shuang, C.; Li, P.; Li, A.; Zhou, Q.; Zhang, M.; Zhou, Y. Quaternized Magnetic Microspheres for the Efficient Removal of Reactive Dyes. *Water Res.* **2012**, *46*, 4417−4426.

(14) Saiz, J.; Bringas, E.; Ortiz, I. Functionalized Magnetic Nanoparticles as New Adsorption Materials for Arsenic Removal from Polluted Waters. *J. Chem. Technol. Biotechnol.* **2014**, *89*, 909−918.

(15) Keyhanian, F.; Shariati, S.; Faraji, M.; Hesabi, M. Magnetite Nanoparticles with Surface Modification for Removal of Methyl Violet from Aqueous Solutions. *Arab. J. Chem.* **2016**, *9*, S348−S354.

(16) Auffan, M.; Rose, J.; Proux, O.; Borschneck, D.; Masion, A.; Chaurand, P.; Hazemann, J.-L.; Chaneac, C.; Jolivet, J.-P.; Wiesner, M. R.; et al. Enhanced Adsorption of Arsenic onto Maghemites Nanoparticles: As(III) as a Probe of the Surface Structure and Heterogeneity. *Langmuir* **2008**, *24*, 3215−3222.

(17) Qu, X.; Alvarez, P. J. J.; Li, Q. Applications of Nanotechnology in Water and Wastewater Treatment. *Water Res.* **2013**, *47*, 3931−3946.

(18) Kistler, S. S.; Caldwell, A. G. Thermal Conductivity of Silica Aërogel. *Ind. Eng. Chem.* **1934**, *26*, 658−662.

(19) Pedroso, M.; Flores-Colen, I.; Silvestre, J. D.; Gomes, M. G.; Silva, L.; Ilharco, L. Physical, Mechanical, and Microstructural Characterisation of an Innovative Thermal Insulating Render Incorporating Silica Aerogel. *Energy Build.* **2020**, *211*, No. 109793.

(20) Vareda, J. P.; Valente, A. J. M.; Durães, L. Silica Aerogels/Xerogels Modified with Nitrogen-Containing Groups for Heavy Metal Adsorption. *Molecules* **2020**, *25*, 15−19.

(21) Amonette, J. E.; Matyáš, J. Functionalized Silica Aerogels for Gas-Phase Purification, Sensing, and Catalysis: A Review. *Microporous Mesoporous Mater.* **2017**, *250*, 100−119.

(22) Rajanna, S. K.; Kumar, D.; Vinjamur, M.; Mukhopadhyay, M. Silica Aerogel Microparticles from Rice Husk Ash for Drug Delivery. *Ind. Eng. Chem. Res.* **2015**, *54*, 949−956.

(23) Dhukate, A. K.; Mullani, S. B.; Dennany, L.; Delekar, S. D. Metal Oxide Nanocomposite-Based Electrochemical Biosensing Studies. In *Advances in Metal Oxides and Their Composites for Emerging Applications*; Elsevier, 2022; pp 379−399. DOI: 10.1016/B978-0-323-85705-5.00015-4.
(24) Soleimani Dorcheh, A.; Abbasi, M. H. Silica Aerogel; Synthesis, Properties and Characterization. *J. Mater. Process. Technol.* **2008**, *199*, 10−26.
(25) Maleki, H.; Durães, L. Microporous and Mesoporous Materials Synthesis of Lightweight Polymer-Reinforced Silica Aerogels with Improved Mechanical and Thermal Insulation Properties for Space Applications. *Microporous Mesoporous Mater.* **2014**, *197*, 116−129.
(26) Parmenter, K. E.; Milstein, F. Mechanical Properties of Silica Aerogels. *J. Non-Cryst. Solids* **1998**, *223*, 179−189.
(27) Moner-Girona, M.; Roig, A.; Molins, E.; Martínez, E.; Esteve, J. Micromechanical Properties of Silica Aerogels. *Appl. Phys. Lett.* **1999**, *75*, 653−655.
(28) Moner-Girona, M.; Martínez, E.; Roig, A.; Esteve, J.; Molins, E. Mechanical Properties of Silica Aerogels Measured by Micro-indentation: Influence of Sol-Gel Processing Parameters and Carbon Addition. *J. Non-Cryst. Solids* **2001**, *285*, 244−250.
(29) Venkateswara Rao, A.; Kulkarni, M. M.; Amalnerkar, D. P.; Seth, T. Superhydrophobic Silica Aerogels Based on Methyltrimethoxysilane Precursor. *J. Non-Cryst. Solids* **2003**, *330*, 187−195.
(30) Venkateswara Rao, A.; Bhagat, S. D.; Hirashima, H.; Pajonk, G. M. Synthesis of Flexible Silica Aerogels Using Methyltrimethoxysilane (MTMS) Precursor. *J. Colloid Interface Sci.* **2006**, *300*, 279−285.
(31) Venkateswara Rao, A.; Latthe, S. S.; Nadargi, D. Y.; Hirashima, H.; Ganesan, V. Preparation of MTMS Based Transparent Superhydrophobic Silica Films by Sol-Gel Method. *J. Colloid Interface Sci.* **2009**, *332*, 484−490.
(32) He, S.; Yang, H.; Chen, X. Facile Synthesis of Highly Porous Silica Aerogel Granules and Its Burning Behavior under Radiation. *J. Sol-Gel Sci. Technol.* **2017**, *82*, 407−416.
(33) Li, X.; Yang, Z.; Li, K.; Zhao, S.; Fei, Z.; Zhang, Z. A Flexible Silica Aerogel with Good Thermal and Acoustic Insulation Prepared via Water Solvent System. *J. Sol-Gel Sci. Technol.* **2019**, *92*, 652−661.
(34) Liu, R.; Dong, X.; Xie, S.; Jia, T.; Xue, Y.; Liu, J.; Jing, W.; Guo, A. Ultralight, Thermal Insulating, and High-Temperature-Resistant Mullite-Based Nanofibrous Aerogels. *Chem. Eng. J.* **2019**, *360*, 464−472.
(35) Shafi, S.; Zhao, Y. Superhydrophobic, Enhanced Strength and Thermal Insulation Silica Aerogel/Glass Fiber Felt Based on Methyltrimethoxysilane Precursor and Silica Gel Impregnation. *J. Porous Mater.* **2020**, *27*, 495−502.
(36) Cai, H.; Jiang, Y.; Feng, J.; Zhang, S.; Peng, F.; Xiao, Y.; Li, L.; Feng, J. Preparation of Silica Aerogels with High Temperature Resistance and Low Thermal Conductivity by Monodispersed Silica Sol. *Mater. Des.* **2020**, *191*, No. 108640.
(37) Lu, J.; Da; Xue, J. Poisoning: Kinetics to Therapeutics. In *Critical Care Nephrology*, 3rd ed.; Elsevier, 2019; pp 600−629.
(38) Wu, X.; Li, Z.; Joao, G.; Zhang, Y.; Huang, S.; Liu, Q. Reducing the Flammability of Hydrophobic Silica Aerogels by Tailored Heat Treatment. *J. Nanopart. Res.* **2020**, *22*, No. 83.
(39) Tian, J.; Shafi, S.; Tan, H.; Zhao, Y. Mechanical and Thermal-Insulating Performance of Silica Aerogel Enhanced Jointly with Glass Fiber and Fumed Silica by a Facile Compressing Technique. *Chem. Phys. Lett.* **2020**, *739*, No. 136950.
(40) Liu, B.; Ju, W.; Zhang, J.; Fan, H.; Wang, Q.; Yi, X.; Yu, Z.; Wang, X. Improvement of Mechanical Strength of Ultralight Resorcinol−Formaldehyde/Silica Aerogel by Addition of Zirconia. *J. Sol-Gel Sci. Technol.* **2017**, *83*, 100−108.
(41) Saka, C. BET, TG-DTG, FT-IR, SEM, Iodine Number Analysis and Preparation of Activated Carbon from Acorn Shell by Chemical Activation with ZnCl2. *J. Anal. Appl. Pyrolysis* **2012**, *95*, 21−24.
(42) Bhavsar, K. S.; Labhane, P. K.; Dhake, R. B.; Sonawane, G. H. Solvothermal Synthesis of Activated Carbon Loaded CdS Nanoflowers: Boosted Photodegradation of Dye by Adsorption and Photocatalysis Synergy. *Chem. Phys. Lett.* **2020**, *744*, No. 137202.
(43) Bhavsar, K. S.; Labhane, P. K.; Huse, V. R.; Dhake, R. B.; Sonawane, G. H. Activated Carbon Immobilized WO3 Nanocuboids: Adsorption/Photocatalysis Synergy for the Enhanced Removal of Organic Pollutants. *Inorg. Chem. Commun.* **2020**, *121*, No. 108215.
(44) Bhavsar, K. S.; Labhane, P. K.; Dhake, R. B.; Sonawane, G. H. Crystal Structures, Morphological, Optical, Adsorption, Kinetic and Photocatalytic Degradation Studies of Activated Carbon Loaded BiOBr Nanoplates Prepared by Solvothermal Method. *Inorg. Chem. Commun.* **2019**, *104*, 134−144.
(45) Wang, B.; Zhou, Y.; Lei Li, H. X.; Xu, H.; Sun, Y.; Sun, Y.; Du, Y.; Du, Y.; Wang, Y. In Situ Synthesis of TiO2-Doped Mesoporous Silica from Coal Fly Ash for the Photocatalytic Degradation of Dyes. *Ind. Eng. Chem. Res.* **2018**, *57*, 15632−15637.
(46) Cornelissen, G.; Noort, Van.; Parsons, P. C. M.; Govers, J. R.; Temperature, H. A. J. Dependence of Slow Adsorption and Desorption Kinetics of Organic Compounds in Sediments. *Environ. Sci. Technol.* **1997**, *31*, 454−460.
(47) Giles, C. H.; Smith, D.; Huitson, A. A General Treatment and Classification of the Solute Adsorption Isotherm. *J. Colloid Interface Sci.* **1974**, *47*, 755−765.
(48) Limousin, G.; Gaudet, J. P.; Charlet, L.; Szenknect, S.; Barthès, V.; Krimissa, M. Sorption Isotherms: A Review on Physical Bases, Modeling and Measurement. *Appl. Geochem.* **2007**, *22*, 249−275.
(49) Bayramoglu, G.; Arica, M. Y. Grafting of Regenerated Cellulose Films with Fibrous Polymer and Modified into Phosphate and Sulfate Groups: Application for Removal of a Model Azo-Dye. *Colloids Surf., A* **2021**, *614*, No. 126173.
(50) Arica, T. A.; Kuman, M.; Gercel, O.; Ayas, E. Poly(Dopamine) Grafted Bio-Silica Composite with Tetraethylenepentamine Ligands for Enhanced Adsorption of Pollutants. *Chem. Eng. Res. Des.* **2019**, *141*, 317−327.
(51) Arica, T. A.; Balci, F. M.; Balci, S.; Arica, M. Y. Highly Porous Poly(o-Phenylenediamine) Loaded Magnetic Carboxymethyl Cellulose Hybrid Beads for Removal of Two Model Textile Dyes. *Fibers Polym.* **2022**, *23*, 2838−2854.
(52) Bayramoglu, G.; Burcu Angi, S.; Acikgoz-Erkaya, I.; Yakup Arica, M. Preparation of Effective Green Sorbents Using O. Princeps Alga Biomass with Different Composition of Amine Groups: Comparison to Adsorption Performances for Removal of a Model Acid Dye. *J. Mol. Liq.* **2022**, *347*, No. 118375.
(53) Yadav, S. K.; Singh, D. K.; Sinha, S. Chemical Carbonization of Papaya Seed Originated Charcoals for Sorption of Pb(II) from Aqueous Solution. *J. Environ. Chem. Eng.* **2014**, *2*, 9−19.
(54) Sonawane, G. H.; Patil, S. P.; Shrivastava, V. S. Photocatalytic Degradation of Safranine by ZnO−Bentonite: Photodegradation versus Adsorbability. *J. Inst. Eng. (India): Ser. E* **2017**, *98*, 55−63.
(55) Chen, K.; Feng, Q.; Ma, D.; Huang, X. Hydroxyl Modification of Silica Aerogel: An Effective Adsorbent for Cationic and Anionic Dyes. *Colloids Surf., A* **2021**, *616*, No. 126331.
(56) Fatimah, I.; Purwiandono, G.; Sahroni, I.; Sagadevan, S.; Chun-oh, W.; et al. Recyclable Catalyst of ZnO/SiO 2 Prepared from Salacca Leaves Ash for Sustainable Biodiesel Conversion. *S. Afr. J. Chem. Eng.* **2022**, *40*, 134−143.
(57) Cotoruelo, L. M.; Rodrı, J. J.; et al. Lignin-Based Activated Carbons as Adsorbents For Crystal Violet Removal from Aqueous Solutions. *Environ. Prog. Sustainable Energy* **2012**, *31*, 386−396.
(58) Awadallah-f, A.; Al-muhtaseb, S. A. Removal of Crystal Violet from Wastewater Using Resorcinol-Formaldehyde Carbon Xerogels. *Sep. Sci. Technol.* **2016**, *51*, 403−415.
(59) Patil, S. A.; Kumbhar, P. D.; Satvekar, B. S.; Harale, N. S.; Bhise, S. C.; Patil, S. K.; Sartape, A. S.; Kolekar, S. S.; Anuse, M. A. Adsorption of Toxic Crystal Violet Dye from Aqueous Solution by Using Waste Sugarcane Leaf-Based Activated Carbon: Isotherm, Kinetic and Thermodynamic Study. *J. Iran. Chem. Soc.* **2022**, *19*, No. 2891.

https://doi.org/10.1021/acsomega.3c00552
ACS Omega 2023, 8, 13285−13299